Different enrichment patterns of pedogenic magnetic particles modulated by primary iron-phosphorous input

Juan Ren[1], Xiaoyong Long[1*], Junfeng Ji[2], Vidal Barrón[3], José Torrent[3] , Yong Wang[1], Shiyou Xie[1]

[1]School of Geographical Sciences, Southwest University, Chongqing, China

[2]Institute of Surficial Geochemistry, College of Earth Sciences and Engineering, Nanjing University, Nanjing, China

[3]Departamento de Agronomía, Universidad de Córdoba, Córdoba, Spain

*Corresponding author: Xiaoyong Long (longxy@126.com);

Key Points:

- Iron oxide crystallinity increases monotonically as soil P/Fe decreases
- Ferrimagnets accompanying hematite enrich with acceleration under high P/Fe
- Rapid grain growth of ferrimagnets and transformation into hematite without the protection of proper amount of P

Abstract

Magnetic particles including ferrimagnetic (FM) and antiferromagnetic (AFM) particles are ubiquitous in the surface of Earth and Mars. The FM particles dominating soil magnetism usually coexist or compete with AFM hematite due to their comparable thermodynamic stability. The uncertain correlation can be modulated by phosphorous (P) absorption during aging of precursor amorphous iron (Fe) oxides. We investigated two Ferralsol sequences around a P mining field with comparable content of hematite but contrasting P/Fe ratio. The FM particles accompanying the formation of hematite are enriched stably at accelerating rates under high P/Fe but at unstably even rates under low P/Fe. The FM particles became less abundant and coarser while the iron oxide crystallinity increased monotonically as P/Fe decreased. We attribute it to more rapid grain growth of FM particles and transformation into hematite without P retarding the crystallization of iron oxides.

Plain Language Summary

Iron (Fe) oxide is an important carrier of soil magnetism. On account of the high affinity of phosphate (P) for iron oxides the relationship between them has been highly concerned. We investigated soil samples from a P mining field and its surrounding with significant variation of P/Fe ratio. It indicates the grain sizes and contents of magnetic particles change with the P/Fe and exhibits different growth and enrichment patterns in different P/Fe ranges. Our results reveal P can affect the aggregation and transformation of iron oxides and related magnetic minerals in soils, which is of great significance for understanding the causes of soil magnetism.

1 Introduction

Magnetic particles derived from pedogenic iron oxides are ubiquitous on the surface of Earth and Mars as the weathering product of Fe-bearing minerals [*Christensen et al., 2001*]. The magnetic particles can be divided into ferrimagnetic (FM) and antiferromagnetic (AFM) particles according to magnetic properties. The FM particles mainly including maghemite (Mgh, γ-Fe_2O_3) and magnetite (Mgt, Fe_3O_4) often dominate soil and sediment magnetism although they make little weight contribution to total amount of iron oxides [*Liu et al., 2012*]. The contents and ratios of FM particles with differing sizes have widely been employed as pedogenic indicators in soil survey and paleoclimate reconstruction, especially in the aeolian sediments of Quaternary loess and Tertiary red clay deposited in Chinese Loess Plateau (CLP) [*Mullins, 1977; Liu et al., 2003; Maher, 2011; Maxbauer et al., 2016; Nie et al., 2016*]. On the other, the AFM particles including hematite (Hm, α-Fe_2O_3) and goethite (Gt, α-FeOOH), which are main red-yellow color agents in soils and sediments, can reflect soil moisture and relative humidity of regional climate [*Cornell and Schwtermann, 2003*]. The Hm/(Hm+Gt) ratio has also been extensively referred in soil taxonomy and assisted in the interpretation of nonlinear magnetic response to climate reconstructed by the loess and red clay in past decades [*Xiong and Li, 1987; Balsam et al., 2004; Ji et al., 2004; Liu et al., 2006; Torrent et al., 2006; Nie et al., 2010; Liu et al., 2013; Gao et al., 2018*].

However, the type, genesis and grain size distribution of FM particles with pedogenesis are still under debate due to field work and laboratory synthesis

conducted under contrast climates and variable conditions [*Lovley and Phillips, 1986; Gálvez et al., 1999; Barrón and Torrent, 2002; Liu et al., 2003*]. Nevertheless, the genetic relation between FM and AFM particles has been gradually confirmed with a growing evidence [*Torrent et al., 2006; Long et al., 2015, 2016*], especially after the nanometer FM particles with growing size from superparamagnetic (SP) to single domain (SD) were found to act as intermediate products of Hm in the solution under ambient conditions [*Barrón and Torrent, 2002; Liu et al., 2008; Gutiérrez et al., 2016; Jiang et al., 2018*]. The process has been evidenced by the common positive relation between SP particles and Hm in soils and sediments derived from different parent materials and wide climate range at a large scale, even in the soils with low Hm formation efficiency in high rainfall regions [*Torrent et al., 2006; Long et al., 2015, 2016*]. Moreover, the accumulating rate of fine FM particles accompanying the formation Hm decreases with the formation efficiency of Hm estimated by Hm/(Hm+Gt) due to their grain growth and transformation into Hm [*Long et al., 2015*]. However, the negative correlation between SP particles and Hm can be only found in the tropical soils with extremely high Hm/(Hm+Gt) above 0.6, which suggests the more rapid transformation from FM to AFM particles than the accumulation of FM particles [*Long et al., 2015*]. Furthermore, at a large spatial and temporal scale, the change of FM particles and Hm, which determine magnetism and redness of soils and sediments, change out of phase. For example, the surface soils in south tropical China are characterized by lower magnetism and higher redness than those in north temperate China [*Han et al., 1996; Yang et al., 2001; Hu et al., 2014*].

Similar phenomenon can also be found in the comparison between Tertiary red clay and Quaternary loess on CLP [*Nie et al., 2010, 2016*]. Considering the Hm/(Hm+Gt) of soils and sediments is too low to favor the transformation from FM particles to Hm, the uncertain relation between them at a large scale could be affected by other factors besides climate.

Theoretically, the presence of FM particles as the intermediate product of Hm in solution is attributed to their higher thermodynamic stability relative to Hm at nanometer [*Chernyshova et al., 2007; Navrotsky et al., 2008; Hiemstra, 2015*]. The size-dependent stability can be maintained with anion absorption or ligand exchange to retard grain growth and transformation of FM particles [*Cabello et al., 2009; Jiang et al., 2018*]. Phosphate (P) is widespread in the natural environment and has high affinity for the surface of iron oxides, thereby influencing the crystallization and aggregation of amorphous iron oxide [*Gálvez et al., 1999; Barrón and Torrent, 2002; Wang et al., 2017; Xu et al., 2017; Wang et al., 2018*]. The FM particles can accumulate effectively under a proper P/Fe ratio between 0.025 and 0.0275 during the aging process of Fh in solution with the presence of phosphate [*Barrón and Torrent, 2002*].

However, the effect of P/Fe on the neoformation of FM particles and Hm has not been independently investigated in natural system because the change of P/Fe is often accompanied by chemical weathering that results in the leaching of P and the enrichment of Fe. The competition between Hm and Gt, which occurs extensively in different spatial scale, could also affect the FM particles with Hm [*Cornell and*

105 *Schwtermann, 2003*]. In this study, we focused on two soil sequences around a P
106 mining area under subtropical climate. Each sequence consisting of 3 saprolitic
107 Ferralsol profiles possesses changes of comparable chemical weathering intensity and
108 Hm/(Hm+Gt) but contrast ratio of P/Fe (0.008 ~ 0.179). They provide us an
109 opportunity to explore magnetic enrichment patterns of FM particles accompanying
110 the formation of Hm under different primary Fe and P input from parent material.

111 **2 Materials and Methods**

112 The two soil sequences were sampled around the Kunyang P mining area, which
113 is located at Yunnan Plateau in southwestern China and is one of the largest P mining
114 areas in the world. This mining area is derived from Paleozoic siliceous dolomite
115 strata and contains phosphorite with a P_2O_5 proportion of up to 36% [*Xiao et al.,*
116 *2019*]. The mean altitude of the Yunnan Plateau is around 2000 m, and the climate is
117 relatively dry and warm with a mean annual precipitation of 994 mm and a mean
118 annual temperature of 15.1 °C. All profiles were sampled on a highland with well
119 drainage on both sides. The uppermost soils can be categorized as Ferralsol, which
120 was considered to have undergone strong chemical weathering since the uplift of
121 Yunnan Plateau in Late Cenozoic [*Yin, 2010*]. The soil profiles covered by natural
122 woodlands and grasslands were focused, and the samples were collected from the
123 surface to the bottom of outcrops covering horizons with the intervals of 20 cm or 40
124 cm depending on the thickness of profile.

125 The air-dried soil samples were sieved to < 2 mm and ground into powders to
126 conduct chemical analysis. The chemical compositions were determined by

X-ray fluorescence method using ARL9800XP + XRF spectrometry. The Chemical Index of Alteration (CIA) was calculated as $Al_2O_3/(Al_2O_3 + CaO + Na_2O + K_2O)$. The total Fe ($Fe_t$) and total P ($P_t$) were separately calculated by Fe_2O_3 and P_2O_5 expressed as percentage. The P/Fe was calculated by molar ratio of P and Fe. The free iron (Fe_d) and amorphous iron (Fe_o) were extracted with citrate-bicarbonate-dithionite (CBD) and ammonium oxalate, respectively. Diffuse reflectance spectra (DRS) was measured on a Perkin-Elimer Lambda 900 spectrophotometer at 2 nm intervals. The redness was calculated as the ratio of average reflectance in the red light band (630 ~ 700 nm) and visual light band (400 ~ 700 nm). Standard Hm and Gt minerals used in the experiment were Pfizer R1599 red and Hoover Color Corporation Synox Hy610 yellow. The Hm was estimated by a working curve established by the deferrated samples mixed with a series of given content of standard Hm and Gt according to the procedure in our previous study [*Long et al., 2011*]. Finally, the Hm and Gt content were calculated by the following equation when we assign free iron oxides (Fe_d) to the combination of iron in stoichiometric Hm (Fe_2O_3), Gt (FeOOH) [*Torrent et al., 2007*] and Fe_o:

$$\text{Hm (\%)} = 10^{-4} \times e^{23.03 * \text{Redness}}$$

$$\text{Gt (\%)} = 1.59 \times (Fe_d - Fe_o - \text{Hm}/1.43)$$

Magnetic susceptibility (χ) was measured with a MS2 instrument from Bartington. The low-frequency (χ_{lf}) and high-frequency (χ_{hf}) were determined at 0.47 and 4.7 kHz to estimate the total ferrimagnet content. The frequency dependence of the magnetic susceptibility, χ_{fd} and χ_{fd}%, usually used to estimate the absolute and

relative content of ultra-fine (＜20 nm) SP particles, was defined as $\chi_{lf} - \chi_{hf}$ and ($\chi_{lf} - \chi_{hf}$) / χ_{lf} × 100% respectively [*Dearing et al., 1996*]. Meanwhile, the anhysteretic remanent magnetization (ARM), which is sensitive to SD particles [*Liu et al., 2004*], was measured in an alternating field of 100 mT with a superimposed 0.05 mT bias field. The χ_{ARM} was calculated by ARM normalized by the basing field. The saturation isothermal remanent magnetization (SIRM) was attained at 1T with the ASC-10 impulse magnetizer and measured with an AGICO JR6 spinner magnetometer.

3 Results

As illustrated in **Table 1 and Figure 1**, the P_t reveals a significant change from 0.07% to 0.85% while the Fe_t changes from 6.3% to 17.7%, which results in the wide range of P/Fe from 0.008 to 0.179 (**Figures 1a and 1b**). According to the P/Fe, the profiles can be divided into HP sequence with high P/Fe (0.037 ~ 0.179) and LP sequence with low P/Fe (0.008 ~ 0.023). These profiles were labeled according to the mean P/Fe following the order HP3 > HP2 > HP1 > LP3 > LP2 > LP1. The ranges of P/Fe in HP and LP sequences are divided by the P/Fe ratio of 0.025 ~ 0.0275 proposed to control the FM particle transformation in solution [*Barrón and Torrent, 2002; Cabello et al., 2009*]. However, the two sequences have undergone comparable chemical weathering as indicated by the CIA from 85.2 to 96.5 in HP sequence, and from 87.3 to 99.2 in LP sequences **(Figure 1b).**

As for the iron oxides, the total amount of pedogenic iron oxides estimated by Fe_d ranging from 4.6% to 10.1% in HP sequence is only slightly lower than that from 5.7% to 12.7% in LP sequence (**Figure 1c**) due to the opposite change of Fe_t and

171 Fe_d/Fe_t (**Figures 1a and 1c**). In contrast, the Fe_o and Fe_o/Fe_d in HP sequence are
172 commonly higher than those in LP sequence (**Figure 1d**). However, the Hm changes
173 from 0.57% to 5.59% in HP sequence and from 0.56% to 8.3% in LP sequence, while
174 Hm/(Hm+Gt) in HP sequence ranging from 0.07 to 0.44 is similar to that from 0.06 to
175 0.49 in LP sequence (**Figure 1e**). Besides, the absolute contents of FM particles
176 indicated by χ_{fd}, χ_{ARM} and SIRM are mostly lower in HP sequence than those of in LP
177 sequence, which accords with the change trend of Fe_d and Hm, but the relative
178 proportions of finer FM particles indicated by χ_{fd}%, χ_{fd}/χ_{ARM}, and ARM/SIRM are
179 significantly higher in HP sequence than in LP sequence (**Figures 1f-1h**).

180 To explore the P/Fe effect on the enrichment of iron oxides and related FM
181 particles, the above parameters were plotted versus P/Fe (**Figure 2**). Note that the
182 P/Fe was plotted in reverse order from high to low indicating chemical weathering
183 from weak to strong in each sequence. These parameters have demonstrated common
184 increase in each sequence except that the P_t and Fe_o/Fe_d reveal monotonic deceasing
185 as P/Fe decreases.

186 **4 Discussion**

187 **4.1 Monotonic increasing crystallinity of iron oxides with the decreasing of P/Fe**

188 The P_t and Fe_t show opposite liner change along two sequences (**Figures 2a and**
189 **2e**), which indicates the loss of P mainly derived from primary P-bearing minerals
190 (mostly apatite) accompanied by the enrichment of immobile iron oxides with
191 enhanced chemical weathering [*Ruttenberg, 2003*]. However, the soils possess lower
192 Fe_t and higher Fe_d/Fe_t in HP sequence than those in LP sequence, which thus narrows

193 the difference of Fe_d, Hm and Gt between both sequences. It could be attributed to the
194 more primary Fe carbonate in LP sequence, which is easier to be weathered than
195 primary Fe silicates in dolomite strata [*Veizer and Mackenzie, 2003*]. Meanwhile, the
196 monotonical decreasing of Fe_o/Fe_d with P/Fe indicates that the crystallinity of iron
197 oxide increases as P/Fe reduces (**Figure 2g**). It confirms the conclusion that presence
198 of phosphate can retard the crystallization or aggregation of amorphous iron oxide in
199 soil solution [*Gálvez et al., 1999; Barrón and Torrent, 2002*].

200 **4.2 Comparable Hm and Gt competition in high and low P/Fe sequences**

201 In contrast to the monotonic change of amorphous iron oxide along two sequences,
202 the competition between crystalline Hm and Gt estimated by Hm/(Hm+Gt) changes
203 comparably as the P/Fe reduces in each sequence (**Figures 2d and 2h**). The highest
204 Hm/(Hm+Gt) often appears in the middle of profile **(Figure 1e)** locating at the
205 highest position of upslope bedside the valley **(Table 1)**. Normally, Hm often forms
206 under dry and warm condition with low water actively while Gt forms under wet and
207 cold condition with high water activity, and the competition between them can be
208 observed in natural systems at different scales [*Cornell and Schwtermann, 2003*].
209 Considering two sequences were sampled with limited horizontal (< 12 km) and
210 vertical space (< 400 m), the climatic difference can be neglected but the water
211 redistribution along a slope and a profile can still make significant variations of
212 Hm/(Hm+Gt). The high Hm/(Hm+Gt) in the middle of upslope profile often
213 correlates with well drainage and low water activity. Reversely, the low Hm/(Hm+Gt)
214 in the downslope profiles, especially in the top and bottom, is often accompanied by

the poor drainage controlled by surface water and groundwater [*Boero and Schwertmann, 1987; Torrent et al., 2010*]. In addition, the high organic matters and rapid biological process on the surface could also lead to the preferential dissolution of Hm but favor the formation of Gt [*Schwertmann, 1971*].

Nevertheless, the Hm/(Hm+Gt) exhibits a correspond increasing with the decreasing of P/Fe in the two sequences. Previous studies have found that the P/Fe of 0 ~ 0.030 under acid condition often favors the formation of Hm rather than Gt, and the effect become more significant with the increasing temperature from 25°C to 100°C [*Gálvez et al., 1999*]. In this study, the soil pH variation is limited from 4 to 6 (not included in this paper) and the mean annual temperature is around 15°C. Meanwhile, the Hm/(Hm+Gt) demonstrates comparable increases as the P/Fe decreases. Therefore, The change of Hm/(Hm+Gt) and P/Fe in both sequence seems to be both controlled by comparable chemical weathering under similar pedogenic environment. In other words, the variation of Hm/(Hm+Gt) in both sequences is mainly controlled by the exterior factor of soil moisture rather than interior factor of parent material composition.

4.3 Different magnetic enhancement patterns in high and low P/Fe sequences

Contrary the comparable change trend of Hm and Gt, the FM particles reveal different change pattern in the two sequences. The FM particles with growing sizes indicated by χ_{fd}, χ_{ARM} and SIRM exhibit common enrichment at stable accelerations (R^2 = 0.90, 0.89 and 0.91) in HP sequence but at unstable even rates (R^2 = 0.53, 0.71 and 0.36) in LP sequence as P/Fe reduces (**Figures 3a-3c**). Meanwhile, the relative

contents of finer FM particles indicated by χ_{fd}% and ARM/SIRM are both higher in HP sequence than those in LP sequence (**Figures 3d and 3f**). However, The χ_{fd}/χ_{ARM} changes comparably but in opposite directions with the decrease of P/Fe. It can be inferred that FM particles accumulated in HP sequence are commonly finer than in LP sequence, but the FM particles around the boundary of SP and SD particles could have undergone significant growth in LP sequence.

4.4 Coordination and Competition between Hm and FM particles in high and low P/Fe sequences

To evaluate the amount and size distribution of FM particles accompanying Hm with the decreasing of P/Fe, the magnetic parameters were normalized by Hm and replotted versus P/Fe. As illustrated in **Figures 3g-3i**, the FM particles accompanying Hm indicated by χ_{fd}/Hm, χ_{ARM}/Hm and SIRM/Hm exhibit similar change trend as χ_{fd}, χ_{ARM} and SIRM in **Figures 3a-3c**. However, the χ_{ARM}/Hm is comparable in both sequences but the χ_{fd}/Hm is mostly higher and the SIRM/Hm is lower in LP sequence. It suggests SD particles are enriched comparably with Hm in two sequences, while the finer and coarser FM particles are enriched in HP and LP sequence, respectively. In addition, the χ_{fd}%/Hm, (χ_{fd}/χ_{ARM})/Hm and (ARM/SIRM)/Hm, which are calculated to trace the relative change of FM in size with the formation of Hm in **Figures 3j-3l**, commonly reveal monotonic decreasing with the decreasing of P/Fe. It reflects the coarsening of FM particles accompanying Hm with lowering interference of phosphate.

4.5 Mechanism and their significance in paleoclimate reconstruction

Previous experimental studies have found that the organic and inorganic ligands play an important role in modulating the aging product of Fh [*Cabello et al., 2009*]. The proper amount of phosphate via specific adsorption or ligand exchange on the surface of Fh can favor the dehydration and rearrangement of Fh to form Hm but inhibit the dissolution of Fh to form Gt [*Barrón et al., 1997; Gálvez et al., 1999; Xu et al., 2017*]. The Mgh-like FM particles with growing size from SP to SD particles were observed as intermediate products [*Liu et al., 2008*] due to their higher thermodynamic stability than Hm in nanometer [*Navrotsky et al., 2008*]. As the Barrón and Torrent [*2002*]'s experiment conducted in wide range of P/Fe, the FM particles are both gradual enrichment as P/Fe decreases above 0.0275 or below 0.025. The magnetism enhancement patterns are divided by a dramatic magnetic reduction as the P/Fe decrease from 0.0275 to 0.025. Our study verifies the P/Fe-mediated processes by assuming that the ratio of P/Fe in solid soils determines the ratio of phosphate and Fh dispersed in soil solution. Although the formation path of Hm is described by three successive steps as Fh $\overset{1}{\rightarrow}$ SP Mgh $\overset{2}{\rightarrow}$ SD Mgh $\overset{3}{\rightarrow}$ Hm in laboratorial experiments [*Barrón and Torrent, 2002*], we believe that the three steps concur in natural systems but develop to different extent under specific condition. The gradual magnetic enhancement with the decreasing P/Fe is determined by Step 1 and Step 2, two steps by promoting the crystallization and aggregation of Fh to form FM particles, thus the decreasing of phosphate favors the crystallization of Fh to Mgh. However, the abrupt magnetic reduction with the decrease of P/Fe from 0.0275 to

0.025 is dominated by Step 2 and Step 3 after a large amount of FM particles have been accumulated through Step 1.

Generally, the two sequences with comparable change of Hm and Gt but contrast range of P/Fe verified that the ratio of Hm/(Hm+Gt) can be used as a reasonable pedogenic environment and paleoclimatic proxy independent of parent materials in a wide spatio-temporal range. It is noteworthy that the P/Fe plays an important role in modulating the FM particles accompanying Hm in formation rate, accumulation and size distribution. In natural system, the change of P/Fe is often controlled by the parent material composition and chemical weathering intensity. The carbonate protolith deposited in marine environment often possesses much higher mean P/Fe around 0.170 than granitic protolith around 0.043 ~ 0.059 although the Fe content in carbonates is much lower than that of granites [*Chen and Wang, 2005*]. It explains the extremely high magnetism of soils in Terra Rossa derived from carbonate [*Grison et al., 2011; Lu et al., 2012*]. In addition, the soils derived from basaltic rocks, which often have a fairly low P/Fe about 0.010 [*Long et al., 2011*] but have the highest Fe [*Chen and Wang, 2005*], can also cause high magnetism as well as the frequently observed FM particle growth and transformation into Hm [*Da Costa et al., 1999; Lu et al., 2008; Long et al., 2015; Liu et al., 2017*]. However, the sedimentary rocks and sediments possess higher variation of P/Fe depending on the depositing environment and chemical weathering intensity. As for the aeolian sediments of loess and red clay on CLP, the P/Fe of loess and paleosol around 0.031 is commonly higher than that of red clay and paleosol in extreme stages like S5 around 0.019 [*Chen et al., 2001*],

which can also be divided by the inflection range around 0.0275 ~ 0.025. Since the composition of aeolian sediments is usually homogeneous [*Guo et al., 2002*], the lower P/Fe is correlated with higher chemical weathering intensity of red clay than loess and paleosol. Thus, when the climate changed gradually from Tertiary to Quaternary, the shift of magnetic enhancement patterns from low P/Fe to high P/Fe mode can lead to the decoupling of magnetism and redness form loess to red clay although the magnetism and redness mostly change in phase in loess or in red clay. Meanwhile, the warmer Tertiary climate and the longer depositing time could also possibly promote more FM particles transformation into Hm [*Barrón and Torrent, 2002; Jiang et al., 2018*], although these factors should exert a gradual rather than abrupt influence on the change of color and magnetism of loess and red clay. Nevertheless, in addition to phosphate, some other inorganic and organic ligands often concur in soils and sediments despite their lower affinity for iron oxides than phosphate [*Cabello et al., 2009*]. These ligands dominating the formation of crystalline iron oxides and related FM particles can change with parent materials, chemical weathering intensity and biological recycling. The P/Fe-modulated magnetic enhancement patterns would help understand the potential influence of parent materials on magnetic particles besides climatic conditions. Conversely, magnetic particles are proved to be the pedogenic sensitive indicators involving in more comprehensive information about pedogenic environment, which is of great significance in paleoenvironment reconstruction and planet exploration.

5 Conclusion

To unravel the role of P/Fe on the geneses and fate of FM particles in associated with AFM Hm in natural systems, two saprolitic soil sequences around a P mining field are examined. The crystallinity of iron oxide increases monotonically with the decreasing of P/Fe while the Hm and Hm/(Hm+Gt) change comparably in HP and LP sequence under similar regional climate and local water activity variation. More importantly, the enrichment of FM particles accompanying Hm stably accelerates as the P/Fe reduces from 0.179 ~ 0.037 in HP sequence, especially for the finer FM particles. However, the enrichment of FM particles accompanying Hm unstably increases at comparable even rates as the P/Fe reduces from 0.023 to 0.008 in LP sequence. The FM particles accompanying Hm became less and coarser in LP sequence than HP sequence. We attributed it to more rapid grain growth of FM particles and transformation into Hm without enough P protection to retard the crystallization of iron oxides.

Acknowledgements

We thank Dr Cai Yunfeng, Xing Dengchun for their help in the laborious field work in mountainous Southwest China. This study was co-supported by the National Natural Science Foundation of China (41877369) and the Natural Science Foundation of Chongqing, China (CSTC2018JCYJAX0456). The original data presented in this paper can be accessed through the public domain repository Zenodo at https://doi.org/10.5281/zenodo.3932444.

346 **Table 1.** Averages of chemical weathering parameters and iron oxides along different P/Fe profiles

Profile/Sequence	Altitude (m)	P_t (%)	Fe_t (%)	P/Fe	CIA	Fe_d (%)	Fe_o (%)	Hm (%)	Fe_d/Fe_t	Fe_o/Fe_d	Hm/(Hm+Gt)	χ_{lf} (10^{-8} m^3 kg^{-1})
HP3	2010	0.67	10.3	0.118	88.5	7.3	0.39	2.83	0.71	0.05	0.27	244
HP2	2256	0.58	9.6	0.117	91.2	6.6	0.55	2.14	0.67	0.09	0.20	836
HP1	2266	0.26	11.0	0.042	95.4	7.8	0.72	3.52	0.71	0.09	0.33	2140
LP3	1976	0.14	14.2	0.018	90.2	7.6	0.35	2.62	0.53	0.05	0.23	914
LP2	1976	0.12	14.2	0.015	94.5	7.8	0.41	3.82	0.55	0.06	0.33	1345
LP1	2158	0.10	16.7	0.011	97.7	11.2	0.41	6.33	0.67	0.04	0.39	2413
HP sequence	2177	0.51	10.3	0.095	91.6	7.2	0.56	2.76	0.69	0.08	0.26	1050
LP sequence	2037	0.12	15.1	0.015	94.1	9.0	0.39	4.30	0.59	0.05	0.31	1576

347

Figure 1. (a) P_t and Fe_t change in opposite direction along the two sequences. **(b)** P/Fe is common higher in HP sequence than LP sequences with comparable chemical weathering indicated by CIA (Chemical Alternation of Index). **(c)** Fe_d is slightly lower in HP sequence than that in LP sequence due to opposite change of Fe_t and Fe_d/Fe_t. **(d and e)** Amorphous iron oxides indicated by Fe_o and Fe_o/Fe_d are both higher in HP sequence while crystalline iron oxides indicated by Hm and Hm/(Hm+Gt) are a little higher in LP sequence. **(f-h)** The absolute magnetic parameters of χ_{lf}, χ_{ARM} and SIRM are a little lower in HP sequence but the relative parameters of χ_{fd}%, χ_{fd}/χ_{ARM} and ARM/SIRM are commonly higher in HP sequence.

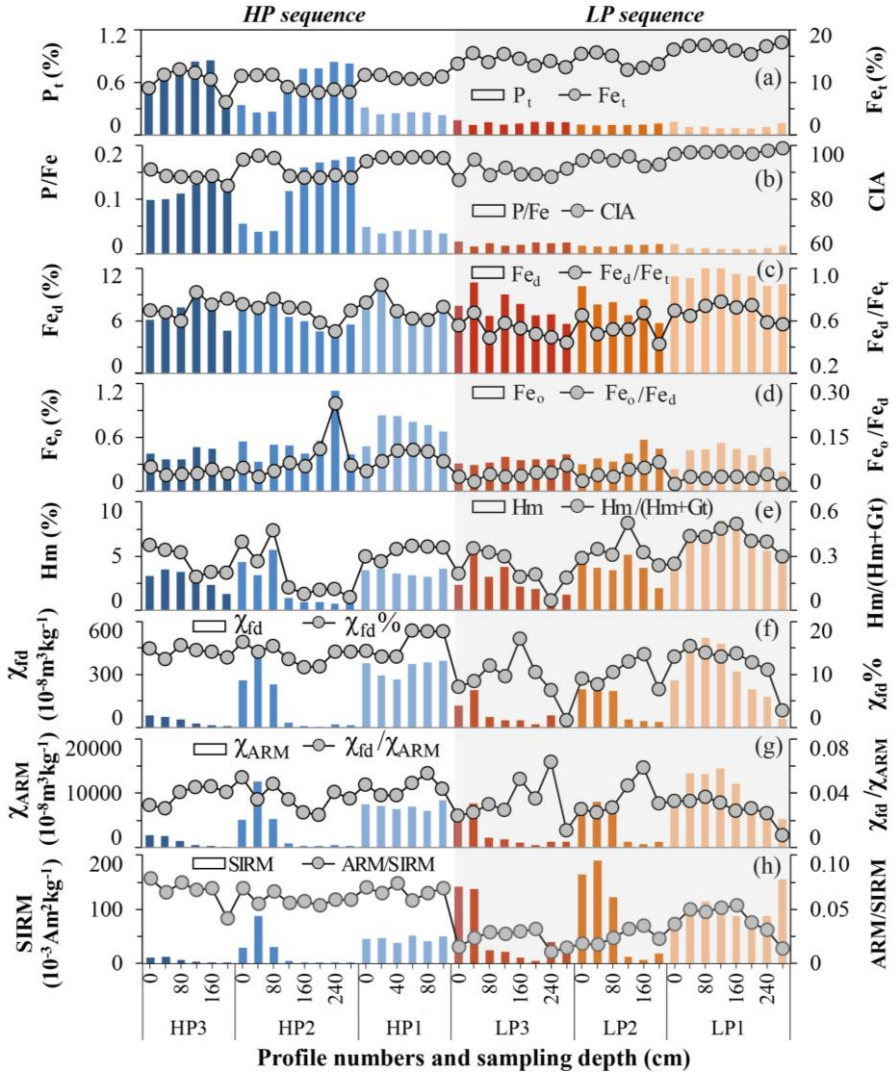

Figure 2. (a and e) P_t and Fe_t monotonously decrease and increase, respectively, with the deceasing of P/Fe in both sequences. **(b-d, f-h)** The Fe_d, Fe_o, Hm and their ratio parameters increase comparably as the P/Fe reduces in two sequences except that the Fe_o/Fe_d decreases monotonously. Note that the x-axis of P/Fe is illustrated in reverse order to indicate chemical weathering from weak to strong. The LP sequence with low P/Fe below 0.025 was shadowed and enlarged independently on the right.

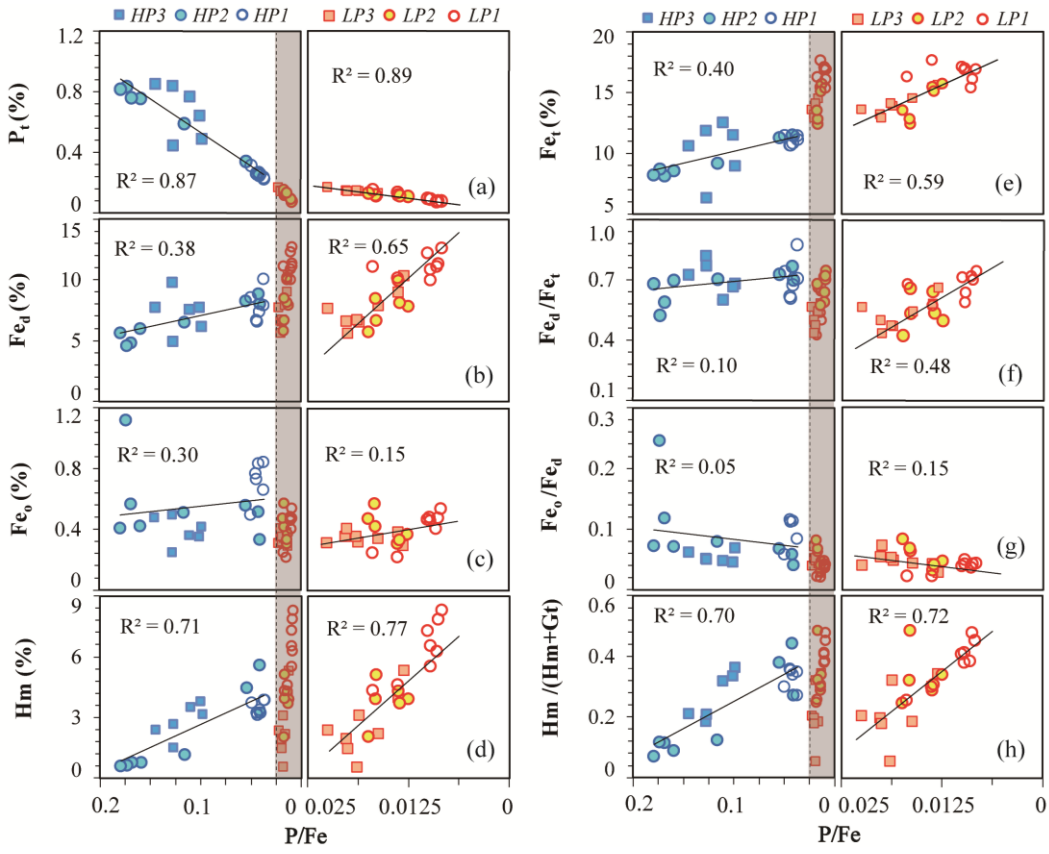

Figure 3. (a-c) The magnetic parameters including χ_{fd}, χ_{ARM} and SIRM increase stably and exponentially in HP sequence but increase unstably and linearly in LP sequence with the decreasing of P/Fe. **(d-f)** The ratios of finer FM particles including χ_{fd}%, χ_{fd}/χ_{ARM} and ARM/SIRM change slowly in HP sequence but rapidly in LP sequence. **(g-i)** The finer and coarser magnetic particles accompanying the formation of Hm indicated by χ_{fd}/Hm and SIRM/Hm are mostly higher and lower, respectively, in HP sequence than those in LP sequence while the intermediate SD particles are kept comparable. **(j-l**) The relative change of grain size of FM particles accompanying Hm indicated by χ_{fd}%/Hm, (χ_{fd}/χ_{ARM})/Hm and (ARM/SIRM)/Hm decrease monotonously with the decreasing of P/Fe.

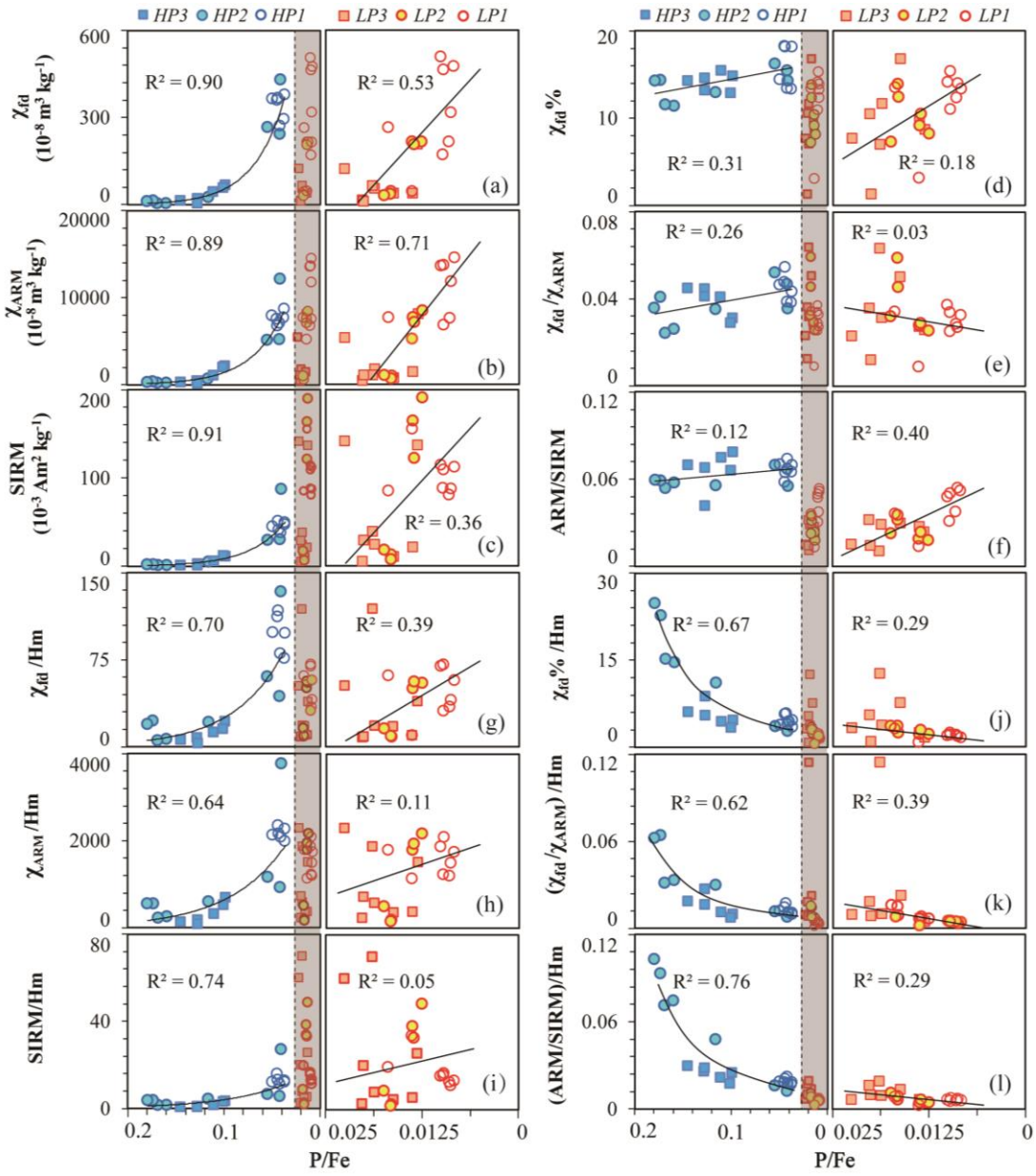
HP3 HP2 HP1 LP3 LP2 LP1
χfd (10-8 m3 kg-1)
R² = 0.90
R² = 0.53
(a)
χARM (10-8 m3 kg-1)
R² = 0.89
R² = 0.71
(b)
SIRM (10-3 Am2 kg-1)
R² = 0.91
R² = 0.36
(c)
χfd /Hm
R² = 0.70
R² = 0.39
(g)
χARM /Hm
R² = 0.64
R² = 0.11
(h)
SIRM/Hm
R² = 0.74
R² = 0.05
(i)
χfd%
R² = 0.31
R² = 0.18
(d)
χfd /χARM
R² = 0.26
R² = 0.03
(e)
ARM/SIRM
R² = 0.12
R² = 0.40
(f)
χfd% /Hm
R² = 0.67
R² = 0.29
(j)
(χfd /χARM) /Hm
R² = 0.62
R² = 0.39
(k)
(ARM/SIRM)/Hm
R² = 0.76
R² = 0.29
(l)
P/Fe

376

References

Balsam, W., J.F. Ji, and J. Chen (2004). Climatic interpretation of the Luochuan and Lingtai loess sections, China, based on changing iron oxide mineralogy and magnetic susceptibility, *Earth and Planetary Science Letters*, *223*(3-4), 335-348. https://doi.org/10.1016/j.epsl.2004.04.023

Barrón, V., N. Gálvez, M.F. Hochella, and J. Torrent (1997). Epitaxial overgrowth of goethite on hematite synthesized in phosphate media: A scanning force and transmission electron microscopy study, *American Mineralogist, 82*(11-12), 1091-1100. https://doi.org/10.2138/am-1997-11-1206

Barrón, V., and J. Torrent (2002). Evidence for a simple pathway to maghemite in Earth and Mars soils, *Geochimica Et Cosmochimica Acta, 66*(15), 2801-2806. https://doi.org/10.1016/S0016-7037(02)00876-1

Boero, V., and U. Schwertmann (1987). Occurrence and transformations of iron and manganese in a colluvial Terra Rossa toposequence of Northern Italy, *Catena*, *14*(6), 519-531. https://doi.org/10.1016/0341-8162(87)90003-8

Cabello, E., M.P. Morales, C.J. Serna, V. Barrón, and J. Torrent (2009). Magnetic enhancement during the crystallization of ferrihydrite at 25 and 50 degrees C, *Clays and Clay Minerals*, *57*(1), 46-53. https://doi.org/10.1346/Ccmn.2009.0570105

Chen, J., Z.S. An, L.W. Liu, J.F. Ji, J.D. Yang, and Y. Chen (2001). Variations in chemical compositions of the eolian dust in Chinese Loess Plateau over the past 2.5 Ma and chemical weathering in the Asian inland, *Science in China Series D-Earth Sciences*, *44*(5), 403-413. https://doi.org/10.1007/Bf02909779

Chen, J., and H.N. Wang (2005) Geochemistry, Science Press, Beijing, 418 pp.

Chernyshova, I.V., M.F. Hochella, and A.S. Madden (2007). Size-dependent structural transformations of hematite nanoparticles. 1. Phase transition, *Physical Chemistry Chemical Physics*, *9*(14), 1736-1750. https://doi.org/10.1039/b618790k

Christensen, P.R., R.V. Morris, M.D. Lane, J.L. Bandfield, and M.C. Malin (2001). Global mapping of Martian hematite mineral deposits: Remnants of water-driven processes on early Mars, *Journal of Geophysical Research-Planets*, *106*(E10), 23873-23885. https://doi.org/10.1029/2000je001415

Cornell, R.M., and U. Schwtermann (2003) The Iron Oxides: Structure, properties, reactions, occurrences and uses, Wiley-VCH Verlag GmbH & Co.KGaA, Weinheim, 661 pp.

Da Costa, A.C.S., J.M. Bigham, F.E. Rhoton, and S.J. Traina (1999). Quantification and characterization of maghemite in soils derived from volcanic rocks in southern Brazil, *Clays and Clay Minerals*, *47*(4), 466-473. https://doi.org/10.1346/Ccmn.1999.0470408

Dearing, J.A., R.J.L. Dann, K. Hay, J.A. Lees, P.J. Loveland, B.A. Maher, and K. OGrady (1996). Frequency-dependent susceptibility measurements of environmental materials, *Geophysical Journal-Oxford, 124*(1), 228-240.

https://doi.org/10.1111/j.1365-246X.1996.tb06366.x
Gálvez, N., V. Barrón, and J. Torrent (1999). Effect of phosphate on the crystallization of hematite, goethite, and lepidocrocite from ferrihydrite, *Clays and Clay Minerals*, *47*(3), 304-311. https://doi.org/10.1346/Ccmn.1999.0470306
Gao, X.B., Q.Z. Hao, L. Wang, F. Oldfield, J. Bloemendal, C.L. Deng, Y. Song, J.Y. Ge, H.B. Wu, B. Xu, F.J. Li, L. Han, Y. Fu, and Z.T. Guo (2018). The different climatic response of pedogenic hematite and ferrimagnetic minerals: Evidence from particle-sized modern soils over the Chinese Loess Plateau, *Quaternary Science Reviews*, *179*, 69-86. https://doi.org/10.1016/j.quascirev.2017.11.011
Grison, H., E. Petrovský, N. Jordanova, and A. Kapička (2011). Strongly magnetic soil developed on a non-magnetic rock basement: A case study from NW Bulgaria, *Studia Geophysica Et Geodaetica*, *55*(4), 697-716. https://doi.org/10.1007/s11200-009-0489-5
Guo, Z.T., W.F. Ruddiman, Q.Z. Hao, H.B. Wu, Y.S. Qiao, R.X. Zhu, S.Z. Peng, J.J. Wei, B.Y. Yuan, and T.S. Liu (2002). Onset of Asian desertification by 22 Myr ago inferred from loess deposits in China, *Nature*, *416*(6877), 159-163. https://doi.org/10.1038/416159a
Gutiérrez, L., V. Barrón, M. Andrés-Vergés, C.J. Serna, S. Veintemillas-Verdaguer, M.P. Morales, and F.J. Lázaro (2016). Detailed magnetic monitoring of the enhanced magnetism of ferrihydrite along its progressive transformation into hematite, *Journal of Geophysical Research-Solid Earth*, *121*(6), 4118-4129. https://doi.org/10.1002/2016jb013016
Han, J.M., H.Y. Lu, N.Q. Wu, and Z.T. Guo (1996). The magnetic susceptibility of modern soils in China and its use for paleoclimate peconstruction, *Studia Geophysica Et Geodaetica*, *40*(3), 262-275. https://doi.org/10.1007/Bf02300742
Hiemstra, T. (2015). Formation, stability, and solubility of metal oxide nanoparticles: Surface entropy, enthalpy, and free energy of ferrihydrite, *Geochimica Et Cosmochimica Acta*, *158*, 179-198. https://doi.org/10.1016/j.gca.2015.02.032
Hu, X.F., Y. Du, C.L. Guan, Y. Xue, and G.L. Zhang (2014). Color variations of the Quaternary Red Clay in southern China and its paleoclimatic implications, *Sedimentary Geology*, *303*, 15-25. https://doi.org/10.1016/j.sedgeo.2014.01.006
Ji, J.F., J. Chen, W. Balsam, H.Y. Lu, Y.B. Sun, and H.F. Xu (2004). High resolution hematite/goethite records from Chinese loess sequences for the last glacial-interglacial cycle: Rapid climatic response of the East Asian Monsoon to the tropical Pacific, *Geophysical Research Letters*, *31*(3), L03207. https://doi.org/10.1029/2003gl018975
Jiang, Z.X., Q.S. Liu, A.P. Roberts, V. Barrón, J. Torrent, and Q. Zhang (2018). A new model for transformation of ferrihydrite to hematite in soils and sediments, *Geology*, *46*(11), 987-990. https://doi.org/10.1130/G45386.1
Liu, Q.S., V. Barrón, J. Torrent, S.G. Eeckhout, and C.L. Deng (2008). Magnetism of intermediate hydromaghemite in the transformation of 2-line ferrihydrite into hematite and its paleoenvironmental implications, *Journal of Geophysical*

Research-Solid Earth, *113*(B1), B01103. https://doi.org/10.1029/2007jb005207

Liu, Q.S., J. Bloemendal, J. Torrent, and C.L. Deng (2006). Contrasting behavior of hematite and goethite within paleosol S5 of the Luochuan profile, Chinese Loess Plateau, *Geophysical Research Letters*, *33*(20), L20301. https://doi.org/10.1029/2006gl027172

Liu, Q.S., M.J. Jackson, Y.J. Yu, F.H. Chen, C.L. Deng, and R.X. Zhu (2004). Grain size distribution of pedogenic magnetic particles in Chinese loess/paleosols, *Geophysical Research Letters*, *31*(22), L22603. https://doi.org/10.1029/2004gl021090

Liu, Q.S., A.P. Roberts, J.C. Larrasoana, S.K. Banerjee, Y. Guyodo, L. Tauxe, and F. Oldfield (2012). Environmental Magnetism: Principles and Applications, *Reviews of Geophysics*, *50*, RG4002. https://doi.org/10.1029/2012rg000393

Liu, X.M., T. Rolph, Z.S. An, and P. Hesse (2003). Paleoclimatic significance of magnetic properties on the Red Clay underlying the loess and paleosols in China, *Palaeogeography Palaeoclimatology Palaeoecology*, *199*(1-2), 153-166. https://doi.org/10.1016/S0031-0182(03)00504-2

Liu, Z.F., Q.S. Liu, J. Torrent, V. Barrón, and P.X. Hu (2013). Testing the magnetic proxy χ_{FD}/HIRM for quantifying paleoprecipitation in modern soil profiles from Shaanxi Province, China, *Global and Planetary Change*, *110*, 368-378. https://doi.org/10.1016/j.gloplacha.2013.04.013

Liu, Z.F., J.L. Ma, G.J. Wei, Q.S. Liu, Z.X. Jiang, X. Ding, S.S. Peng, T. Zeng, and T.P. Ouyang (2017). Magnetism of a red soil core derived from basalt, northern Hainan Island, China: Volcanic ash versus pedogenesis, *Journal of Geophysical Research-Solid Earth*, *122*(3), 1677-1696. https://doi.org/10.1002/2016jb013834

Long, X.Y., J.F. Ji, and W. Balsam (2011). Rainfall-dependent transformations of iron oxides in a tropical saprolite transect of Hainan Island, South China: Spectral and magnetic measurements, *Journal of Geophysical Research-Earth Surface*, *116*, F03015. https://doi.org/10.1029/2010jf001712

Long, X.Y., J.F. Ji, W. Balsam, V. Barrón, and J. Torrent (2015). Grain growth and transformation of pedogenic magnetic particles in red Ferralsols, *Geophysical Research Letters*, *42*(14), 5762-5770. https://doi.org/10.1002/2015gl064678

Long, X.Y., J.F. Ji, V. Barrón, and J. Torrent (2016). Climatic thresholds for pedogenic iron oxides under aerobic conditions: Processes and their significance in paleoclimate reconstruction, *Quaternary Science Reviews*, *150*, 264-277. https://doi.org/10.1016/j.quascirev.2016.08.031

Lovley, D.R., and E.J.P. Phillips (1986). Organic-Matter Mineralization with Reduction of Ferric Iron in Anaerobic Sediments, *Applied and Environmental Microbiology*, *51*(4), 683-689. https://doi.org/10.1128/Aem.51.4.683-689.1986

Lu, S.G., D.J. Chen, S.Y. Wang, and Y.D. Liu (2012). Rock magnetism investigation of highly magnetic soil developed on calcareous rock in Yun-Gui Plateau, China: Evidence for pedogenic magnetic minerals, *Journal of Applied Geophysics*, *77*, 39-50. https://doi.org/10.1016/j.jappgeo.2011.11.008

Lu, S.G., Q.F. Xue, L. Zhu, and J.Y. Yu (2008). Mineral magnetic properties of a weathering sequence of soils derived from basalt in Eastern China, *Catena*, *73*(1), 23-33. https://doi.org/10.1016/j.catena.2007.08.004

Maher, B.A. (2011). The magnetic properties of Quaternary aeolian dusts and sediments, and their palaeoclimatic significance, *Aeolian Research*, *3*(2), 87-144. https://doi.org/10.1016/j.aeolia.2011.01.005

Maxbauer, D.P., J.M. Feinberg, and D.L. Fox (2016). Magnetic mineral assemblages in gills and paleosols as the basis for paleoprecipitation proxies: A review of magnetic methods and challenges, *Earth-Science Reviews*, *155*, 28-48. https://doi.org/10.1016/j.earscirev.2016.01.014

Mullins, C.E. (1977). Magnetic-susceptibility of soil and its significance in soil science - review, *Journal of Soil Science*, *28*(2), 223-246. https://doi.org/10.1111/j.1365-2389.1977.tb02232.x

Navrotsky, A., L. Mazeina, and J. Majzlan (2008). Size-driven structural and thermodynamic complexity in iron oxides, *Science*, *319*(5870), 1635-1638. https://doi.org/10.1126/science.1148614

Nie, J.S., Y.G. Song, and J.W. King (2016). A review of recent advances in Red-Clay environmental magnetism and paleoclimate history on the Chinese Loess Plateau, *Frontiers in Earth Science*, *4*. https://doi.org/10.3389/feart.2016.00027

Nie, J.S., Y.G. Song, J.W. King, X.M. Fang, and C. Heil (2010). HIRM variations in the Chinese red-clay sequence: Insights into pedogenesis in the dust source area, *Journal of Asian Earth Sciences*, *38*(3-4), 96-104. https://doi.org/10.1016/j.jseaes.2009.11.002

Ruttenberg, K.C. (2003) The global phosphorus cycle, Treatise on Geochemistry 8, Elsevier Inc 585-643 pp.

Schwertmann, U. (1971). Transformation of hematite to goethite in soils, *Nature*, *232*(5313), 624-625. https://doi.org/10.1038/232624a0

Torrent, J., V. Barrón, and Q.S. Liu (2006). Magnetic enhancement is linked to and precedes hematite formation in aerobic soil, *Geophysical Research Letters*, *33*(2), L02401. https://doi.org/10.1029/2005gl024818

Torrent, J., Q.S. Liu, and V. Barrón (2010). Magnetic susceptibility changes in relation to pedogenesis in a Xeralf chronosequence in northwestern Spain, *European Journal of Soil Science*, *61*(2), 161-173. https://doi.org/10.1111/j.1365-2389.2009.01216.x

Torrent, J., Q.S. Liu, J. Bloemendal, and V. Barrón (2007). Magnetic enhancement and iron oxides in the upper luochuan Loess-paleosol sequence, Chinese Loess plateau, *Soil Science Society of America Journal*, *71*(5), 1570-1578. https://doi.org/10.2136/sssaj2006.0328

Veizer, J., and F.T. Mackenzie (2003) Evolution of Sedimentary Rocks, Treatise on Geochemistry 7, 369-407 pp.

Wang, L.J., C.V. Putnis, J. Hovelmann, and A. Putnis (2018). Interfacial precipitation of phosphate on hematite and goethite, *Minerals*, *8*(5), 207. https://doi.org/10.3390/min8050207

552 Wang, X.M., Y.F. Hu, Y.D. Tang, P. Yang, X.H. Feng, W.Q. Xu, and M.Q. Zhu (2017).
553 Phosphate and phytate adsorption and precipitation on ferrihydrite surfaces,
554 *Environmental Science-Nano*, *4*(11), 2193-2204.
555 https://doi.org/10.1039/c7en00705a
556 Xiao, Z., G.F. Chen, J.T. Pang, and H.R. Yu (2019). Analysis of occurrence state of Cr
557 in phosphate rock of Kunyang Phosphate Mine, *Industrial Minerals &*
558 *Processing*, *48*(7), 36-39. https://doi.org/10.16283/j.cnki.hgkwyjg
559 Xiong, Y., and Q.K. Li (1987) Soil in China, Science Press, Beijing, 746 pp.
560 Xu, C.Y., R.K. Xu, J.Y. Li, and K.Y. Deng (2017). Phosphate-induced aggregation
561 kinetics of hematite and goethite nanoparticles, *Journal of Soils and Sediments*,
562 *17*(2), 352-363. https://doi.org/10.1007/s11368-016-1550-y
563 Yang, S.L., X.M. Fang, J.J. Li, Z.S. An, S.Y. Chen, and H. Fukusawa (2001).
564 Transformation functions of soil color and climate, *Science in China Series*
565 *D-Earth Sciences*, *44*, 218-226. https://doi.org/10.1007/Bf02911990
566 Yin, A. (2010). Cenozoic tectonic evolution of Asia: A preliminary synthesis,
567 *Tectonophysics*, *488*(1-4), 293-325. https://doi.org/10.1016/j.tecto.2009.06.002
568